Research paper manuscript submitted to Electrochimica Acta

RH13-058-R1

Remarkable Effect of Bromide Ion upon Two-Dimensional Faradaic Phase Transition of Dibenzyl Viologen on an HOPG Electrode Surface: Emergence of Two-Step Transition

Tomohiro Higashi† and Takamasa Sagara‡*

† Department of Science and Technology, Graduate School of Engineering, Nagasaki University, Bunkyo 1-14, Nagasaki 852-8521, Japan

‡ Division of Chemistry and Materials Science, Graduate School of Engineering, Nagasaki University, Bunkyo 1-14, Nagasaki 852-8521, Japan

*Corresponding author. Tel. & fax: +81 95 8192676;

E-mail address: sagara@nagasaki-u.ac.jp (Takamasa Sagara)

Graphical Abstract (for review)

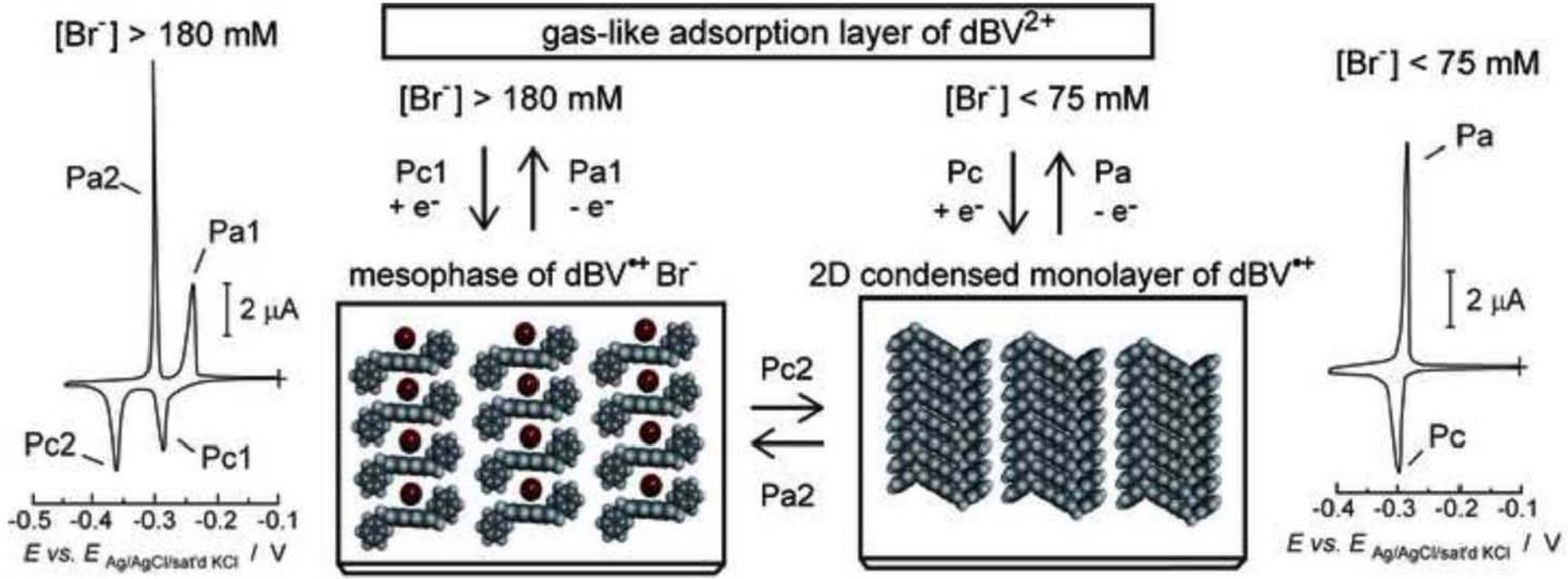

Highlights

► First order faradaic phase transition of dibenzyl viologen (dBV) at HOPG was studied.

► At high Br^- concentration, dBV exhibits two-step phase transitions.

► As the first reduction step, a $dBV^{\bullet+}$ Br^- mesophase emerges at $[Br^-] > 75$ mM.

► As the second, phase transition from the mesophase to a 2D condensed phase occurs.

► Remarkable effect of Br^- upon the transition enabled us to model the mesophase.

Abstract

We found that dibenzyl viologen (dBV) on an HOPG electrode undergoes a two-step first order faradaic phase transition at high concentrations of bromide ion (Br^-). Results of voltammetric and electroreflectance measurements were used to describe the mechanism of the two-step transition processes. When [Br^-] > 180 mM, the transition step at less negative potential was ascribed to a phase transition between a gas-like adsorption layer of dBV dication (dBV^{2+}) and a mesophase of dBV radical cation ($dBV^{\bullet+}$). Most likely, the mesophase is a two-dimensional (2D) ordered phase composed of co-adsorbed $dBV^{\bullet+}$ and Br^- where both are in direct contact with the HOPG surface. The transition step at more negative potential was ascribed to a phase transition between the $dBV^{\bullet+}$ Br^- mesophase and a 2D condensed phase of $dBV^{\bullet+}$. In the condensed phase being denser than the mesophase, $dBV^{\bullet+}$ molecules are π-stacked due to face-to-face interaction between bipyridinium radical cations. This transition step involves also a reduction process of dBV^{2+} to $dBV^{\bullet+}$ followed by its incorporation into the condensed phase. The two-step transition was not observed in KCl solution of any concentration, either in KBr solution of [Br^-] < 75 mM. Other viologens examined, including benzyl-heptyl viologen, did not exhibit such a two-step transition but single-step one. The nature of the transition, especially in the [Br^-] range from 75 to 180 mM, was closely analyzed.

Keywords: Viologen; HOPG; Phase transition; Anion effect; Electroreflectance

1. Introduction

Viologens are among the representative organic redox species which undergo a faradaic phase transition of the first order on a highly oriented pyrolytic graphite (HOPG) electrode [1-8]. Phase transitions of dialkyl viologens [1-7] and dibenzyl viologen (dBV) [8] so far studied at an HOPG electrode in aqueous media are characterized by one anodic and one cathodic spike-like sharp peaks in dc voltammograms. These are of a single-step first order phase transition between a gas-like adsorption layer of viologen dication (V^{2+}) and an insoluble two-dimensional (2D) condensed monolayer of radical cation ($V^{\bullet+}$). In the transitions at an HOPG electrode, any stable mesophase of viologen has not been found in between the above mentioned two phases. Known exceptions have been so far found only at metal electrodes [9-17].

Recently, we have discovered the occurrence of a two-step phase transition at a HOPG electrode for dBV in the presence of high concentrations of Br^- showing two-consecutive sharp spike-like peaks in cyclic voltammograms (CVs) in both scans in negative and positive directions. We herein report this discovery for the first time, together with the results of in-depth studies of the transition mechanisms and the roles played by coexistent Br^-. Results of voltammetric and electroreflectance (ER) measurements were used to clarify the nature of the mesophase.

Among the potential driven phase transitions of two-dimensional (2D) adlayers at electrified interfaces, metal underpotential deposition (UPD) processes often occur in multiple steps. As a typical example, Cu-UPD onto an Au(111) in sulfate solution exhibits two consecutive sharp peaks in CVs [18,19]. This UPD process was fully understood as a two-step transition. The first step is the formation of a honeycomb lattice structure of a Cu sub-monolayer, and the second is the transformation to a commensurate full monolayer of Cu. Significant effects of halide ions in solution phase on this two-step UPD process have been highlighted [19]. However, irrespective of Cl^- or Br^- concentrations, the UPD process is always of two-step. In sharp contrast, the phase transition of dBV of our interest is highly susceptible to Br^- concentration.

As for viologens on metal electrodes, a few examples of multi-step transitions have been known. Millán and co-workers found a two-step phase transition of heptyl viologen (HV) on an Hg electrode in (water + DMSO) mixed solution of KBr [13]. They interpreted the first step, upon the potential scan to negative direction, as a one-electron reduction process of weakly adsorbed HV^{2+} to form a 2D condensed $HV^{\bullet+}$ Br^- layer with a flat-lying orientation in face-on

configuration. They interpreted the second step as a reorientation process of $HV^{\bullet+}$ Br^- from face-on to side-on configuration, accompanied by additional incorporation of reduction product $HV^{\bullet+}$ molecules from solution. Arihara and Kitamura reported multi-step sharp phase transitions on a Au(111) electrode surface due to structural changes of $HV^{\bullet+}$ adsorption layers [9]. In their model, a face-on bilayer of $HV^{\bullet+}$ was formed at the first step, and then at the second step, the bilayer changed to a more close-packed state. The authors claimed that the transition at the second step involves both additional reduction process of HV^{2+} to $HV^{\bullet+}$ and reorientation of heptyl chains from parallel to nearly normal to the electrode surface.

We previously studied the single-step phase transition of dBV at an HOPG electrode in KCl solution [8]. The condensed phase produced by its single-step first-order transition was analyzed by ER and electrochemical scanning tunneling microscopic (EC-STM) measurements. In the transition, a full monolayer of $dBV^{\bullet+}$ molecules is formed with the flat-lying longitudinal molecular axis of the bipyridinium moiety in a side-on configuration. The face-to-face π-π stacking interactions with nearest neighbor molecules, both between $V^{\bullet+}$ moieties and between side group benzene rings, are the origins of the formation of the π-stacked condensed phase. Regardless of the electrode material, π-π stacking interaction with the nearest neighbor $V^{\bullet+}$ moieties plays a central role in the ordered condensed monolayer formation.

In this paper, we demonstrate Br^- concentration dependent phase transition of dBV in KBr solution with a focus in particular on the 2D condensation process of $dBV^{\bullet+}$ molecules on a HOPG electrode. The results of this study may provide us with the new physical insight into the 2D assembling behavior of organic molecules at electrified interface together with the roles played by the counter anion upon the transition.

2. Experimental

2.1. Materials

Dibenzyl viologen dichloride (1,1'-dibenzyl-4,4'-bipyridinium dichloride: dBV^{2+} $2Cl^-$) purchased from Tokyo Chemical Industry Co. (TCI) was recrystallized from acetone + ethanol and dried in vacuo. Dibenzyl viologen dibromide (1,1'-dibenzyl-4,4'-bipyridinium dibromide: dBV^{2+} $2Br^-$) was prepared through Menshutkin reaction by heating the mixture of 4,4'-bipyridine

(TCI, 3.0 mmol) and benzyl bromide (TCI, 8.3 mmol) in dry DMF (10 mL) under N_2 gas atmosphere (70°C, 24 h). Resulting precipitate was washed with acetone and recrystallized from ethanol to obtain the product as yellow crystals with 74 % yield. Benzyl-heptyl viologen (1-benzyl-1'-heptyl-4,4'-bipyridinium dibromide: BHV^{2+} $2Br^-$) was prepared through Menshutkin reaction by heating the mixture of 1-heptyl-4-(4-pyridyl)-pyridinium bromide (Sigma Aldrich, 1.5 mmol) and benzyl bromide (TCI, 3.1 mmol) in dry DMF (6 mL) under N_2 gas atmosphere (80°C, 36 h). Resulting precipitate was washed with acetone and recrystallized from ethanol to obtain the product as yellow crystals with 43 % yield. Water was purified through a Milli-Q integral (Millipore) to a resistivity over 18 MΩ cm. All other reagent chemicals were of the highest grade commercially available and used as received. A plate of HOPG (Matsushita Electric Co., Panasonic graphite, PGX 04: size 12 × 12 × 3 mm-thickness) was connected perpendicularly with a copper pipe using a colloidal graphite paste. To expose a fresh basal plane, the surface of the HOPG was peeled off by the use of Scotch® adhesive tape immediately before use.

2.2. Voltammetric and Electroreflectance (ER) Measurements

For the measurements of CVs, a potentiostat (HUSOU, HECS-9094) was coupled with a function generator (HUSOU, HECS-321B). Potential-step measurements were made by the use of a potentiostat equipped with a digital universal signal processing unit (HUSOU, HECS-326). Approximately 75 μL portion of 0.1 mM dBV^{2+} $2Cl^-$ (or dBV^{2+} $2Br^-$) solution containing KCl and/or KBr was pipetted to place its droplet on an upward surface of a horizontally set HOPG electrode in a wetted Ar gas atmosphere. A tip of an Ag/AgCl/sat'd KCl reference electrode and an Au wire counter electrode were immersed in the droplet. This "droplet configuration" [3] was used in all voltammetric measurements unless otherwise stated. Voltammetric measurements for 0.1 mM BHV^{2+} $2Br^-$ + 0.30 M KBr solution were also made in the droplet configuration. The active electrode area (A), which is the actual contact area of the HOPG surface to solution, was measured photographically. When an HOPG electrode was found to have a greater double-layer capacity over 20 μF cm^{-2}, we ceased its use and reverted back to the peeling-off procedure.

Measurements of ER signals were carried out by normal incidence of monochromatic light at a hanging-meniscus (H-M) configuration. This configuration was set by horizontal touching of

the downward-facing basal plane of a HOPG electrode to an Ar gas | dBV solution interface from the Ar gas phase. The details of the ER instrumentation and spectroelectrochemical cell were given in our previous publication [20]. The potential modulation used for ER measurements is described as

$$E = E_{dc} + E_{ac} = E_{dc} + \Delta E_{ac} \exp(j\omega t) \quad (1)$$

where E is the electrode potential, E_{dc} is the dc potential, E_{ac} is the ac potential, ΔE_{ac} is the zero-to-peak ac amplitude, $\omega = 2\pi f$ is the angular frequency (f is the frequency of the potential modulation), t is the time, and $j = \sqrt{-1}$. Phase-sensitive detection of the ac intensity of the reflected light I_{ac} was made by the use of a lock-in amplifier (EG&G 5210). When the response I_{ac} to E_{ac} is linear, I_{ac} has a form of $\Delta I_{ac} \exp[j(\omega t - \phi)]$ where ΔI_{ac} is the zero-to-peak amplitude of I_{ac} and ϕ is the phase of I_{ac} with respect to E_{ac}. The ER signal $(\Delta R/R)_{ER}$ is defined as

$$(\Delta R/R)_{ER} = \Delta I_{ac} \exp(-j\phi) / I_{dc} \quad (2)$$

where I_{dc} is the time averaged dc intensity of the reflected light. An ER spectrum (ERS) is a plot of both real (in-phase to E_{ac}) and imaginary (90° out-of-phase) parts of $(\Delta R/R)_{ER}$ as a function of the incident light wavelength (λ).

All of the electrochemical control was carried out under Ar gas (>99.998 %) atmosphere at room temperature 24 ± 2°C. All the potentials were referenced to an Ag/AgCl/sat'd KCl electrode.

3. Results and discussion

3.1. Phase transition of dBV in 0.30 M KBr solution: Voltammetry

Typical CVs for dBV at an HOPG electrode in 0.30 M KCl and 0.30 M KBr solutions are shown, respectively, in Fig. 1-a and b. In KCl solution (Fig. 1-a), dBV exhibited a sharp cathodic peak (Pc) and a sharp anodic counterpart (Pa) in the potential range of interest. At further more negative potentials, a diffusion-controlled bulk redox reaction was recorded, which

is beyond the scope of this work. The peaks Pc and Pa are due to 2D faradaic phase transition of the first-order between a gas-like adsorption layer of dBV^{2+} and a 2D condensed monolayer of $dBV^{\bullet+}$ [8]. The electrode surface is fully covered with the condensed monolayer at more negative potentials than these transition peaks. No other phase transition peak was found in the voltammograms than this Pc-Pa couple. The phase transition is, therefore, of a single-step. As far as the concentration of KCl (C_{KCl}) as the electrolyte was ranged from 30 to 500 mM, we observed this single-step phase transition of the first-order.

Figure 1 (single column)

Figure 1-b represents a CV at an HOPG electrode in contact with 0.1 mM dBV^{2+} $2Cl^-$ + 0.30 M KBr solution, showing two cathodic peaks (Pc1 and Pc2) and two anodic peaks (Pa1 and Pa2). Two couples of peaks, Pc1-Pa1 and Pc2-Pa2, were identified because: (i) comparison of the peak charges expressed in terms of the molecular amounts per unit area (Γ) assuming one-electron processes always resulted in $\Gamma(Pc1) = \Gamma(Pa1) = (0.7 \pm 0.2) \times 10^{-10}$ mol cm^{-2} and $\Gamma(Pc2) = \Gamma(Pa2) = (1.6 \pm 0.2) \times 10^{-10}$ mol cm^{-2}, and these values of Γ were independent of potential sweep rate (v), and (ii) when the negative scan vertex potential was set at −0.325 V, recorded as the anodic peak was only Pa1 but no trace of Pa2 was found. The sum of Γ of the two different couples, 2.3×10^{-10} mol cm^{-2}, was near to that of the single couple in KCl (Fig. 1-a), $(2.5 \pm 0.1) \times 10^{-10}$ mol cm^{-2}, being consistent with the amount of the adsorbed $dBV^{\bullet+}$ molecules in its 2D condensed monolayer with molecular alignments described in ref. [8] on an HOPG electrode surface in KCl solution. Separate ER spectral measurements for the two couples in Fig. 1-b revealed that both involve $dBV^{\bullet+}/dBV^{2+}$ one-electron redox processes, as will be detailed in section 3.4. It was also revealed that the cathodic peaks in Fig. 1-b were not due to the bulk reduction of soluble dBV^{2+} to $dBV^{\bullet+}$ Br^- deposit on the surface, which in fact occurred around −0.51 V. Taken together, we tentatively interpreted that, in the presence of Br^-, dBV^{2+} undergoes a two-step faradaic phase transition, leading to the formation of a 2D condensed monolayer.

We also examined the use of KF and KI as the electrolyte salt. In KF solution, dBV^{2+} always exhibited a single-step transition. In the presence of I^-, we occasionally obtained CVs showing a two-step transition (see Supporting Information, Fig. S1), but the response was so complicated

Figure 1
Click here to download high resolution image

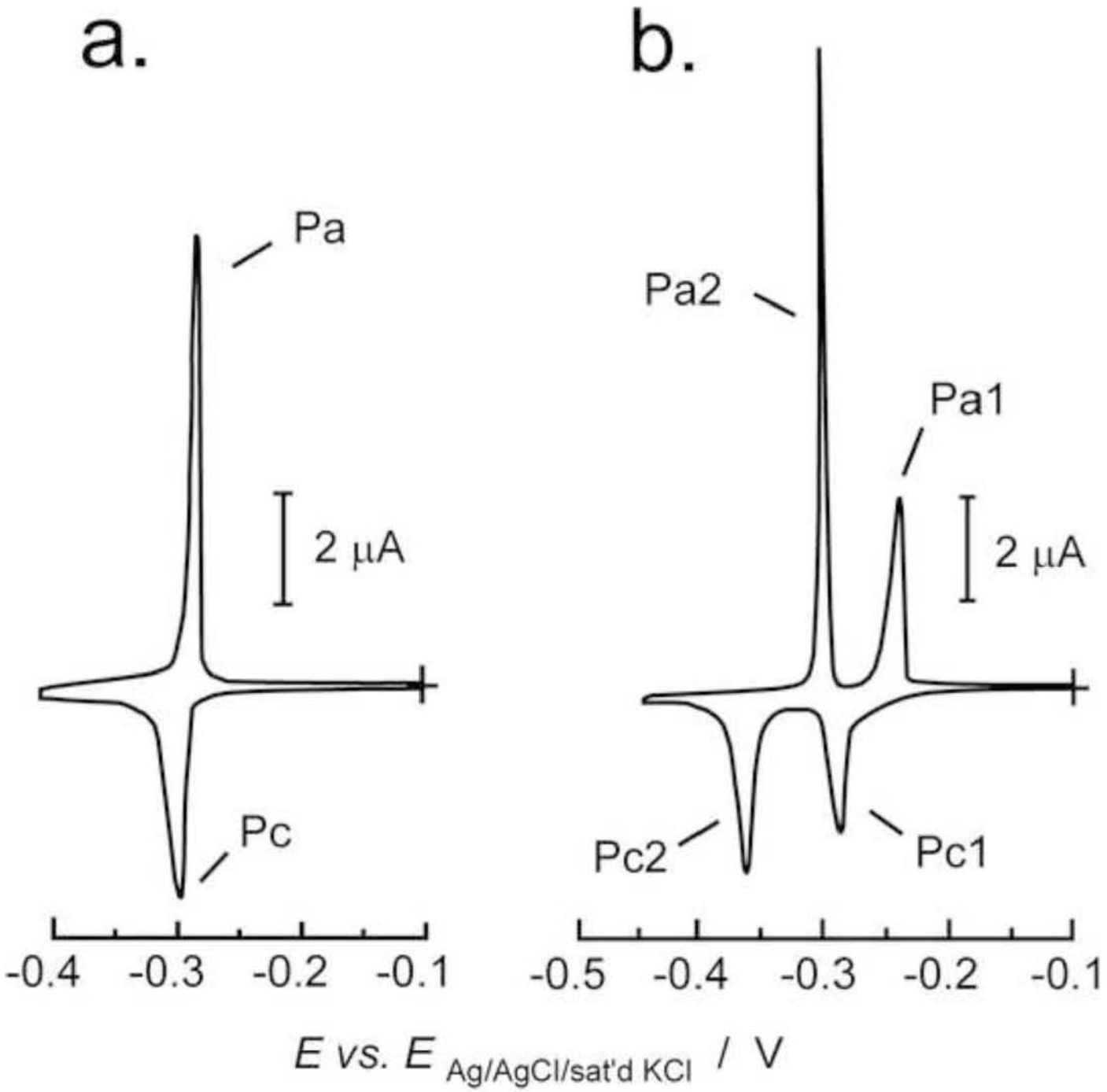

that the condition to realize the two-step transition is still ill-defined. Further study to figure out the conditions is currently underway, and the results will be reported elsewhere.

Figure 2 (single column)

Figure 2 shows the v-dependence of the peak potentials for the CVs in 0.30 M KBr solution. Each of the four peaks converged with constant potentials at v = 0.1 mV s^{-1}. The midpoint potentials ($E_{1/2}$) and the peak separations (ΔE_p) between anodic and cathodic peak potentials were obtained at v = 0.1 mV s^{-1} by $E_{Pj,1/2} = (E_{Pcj} + E_{Paj})/2$ and $\Delta E_{Pj} = E_{Paj} - E_{Pcj}$ with j = 1, 2; $E_{P1,1/2}$ = −268 mV, $E_{P2,1/2}$ = −335 mV, ΔE_{P1} = 28 mV, and ΔE_{P2} = 52 mV. For the single-step transition in 0.30 M KCl, $E_{1/2}$ and ΔE_p at v = 0.1 mV s^{-1} were, respectively, −280 mV and 12 mV [8]. In the first-order phase transition, ΔE_p value at the lower v limit corresponds to the width of the bistable potential region, and the width directly reflects the strength of intermolecular interactions with the nearest neighbors [1-5]. Greater values of the widths in KBr solution compared to that in KCl solution may indicate that the coexistent Br^- enhances attractive interaction between neighboring adsorbed $dBV^{\bullet+}$ molecules.

3.2. Kinetics of the phase transition of dBV in 0.30 M KBr solution

Figure 3 (single column)

The first order phase transitions of the monolayer adsorbed species exhibit nucleation-growth-collision (NGC) kinetic with no exception for viologens on HOPG to our knowledge [1-4,8].

Figure 3 shows the linearity of logarithms of the CV peak current values for the four peaks (Fig. 1-b) to the logarithm of v in the v-range of 10-100 mV s^{-1}. The least squares fitting analysis gave the slopes typed in the figure. The exponents ranging 0.60 to 0.81 were well in accord with a NGC model proposed by Camacho and his colleagues [21]. The same NGC model also applied to the single step phase transition in KCl solution [8].

Figure 2
Click here to download high resolution image

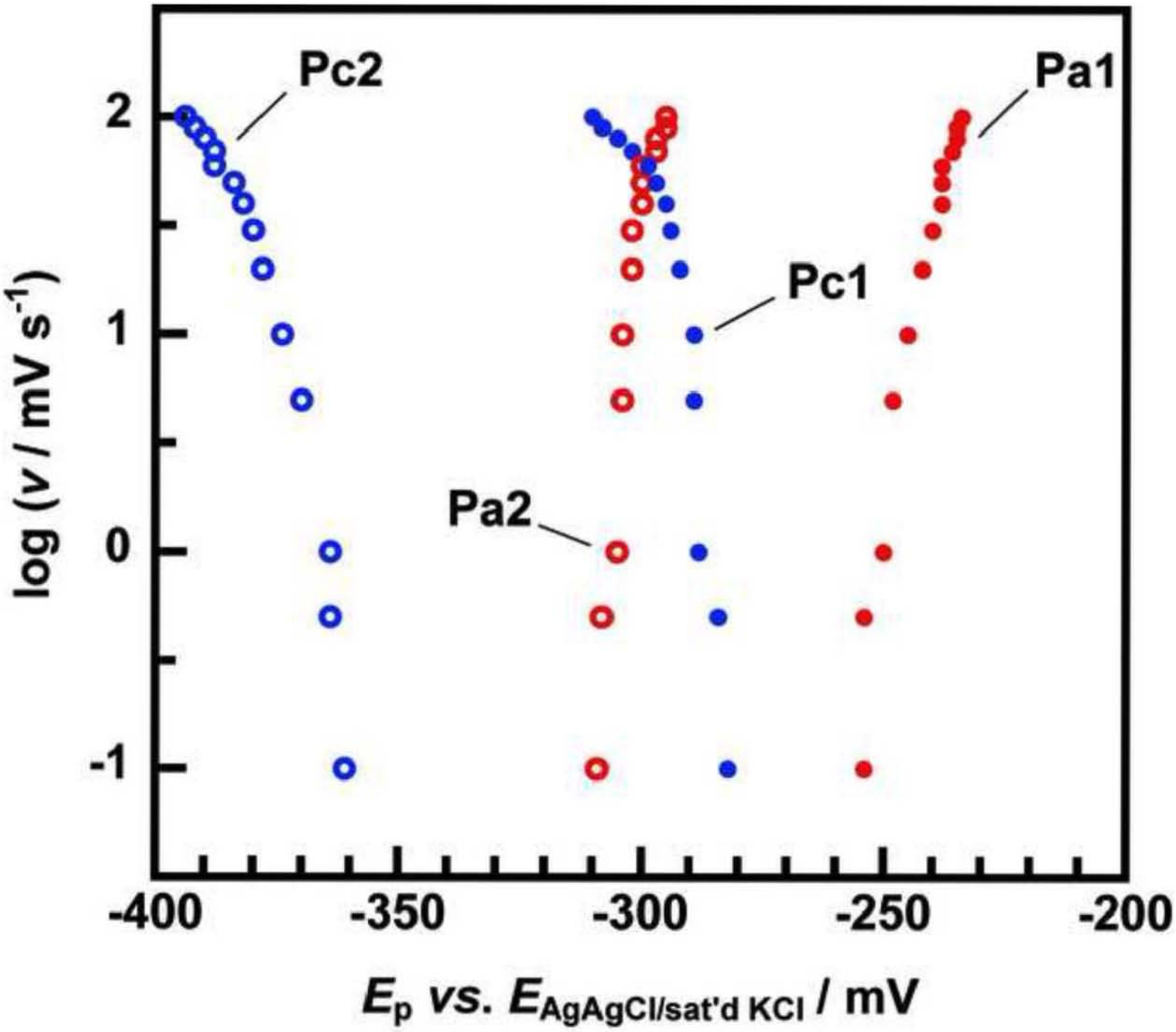

Figure 3
Click here to download high resolution image

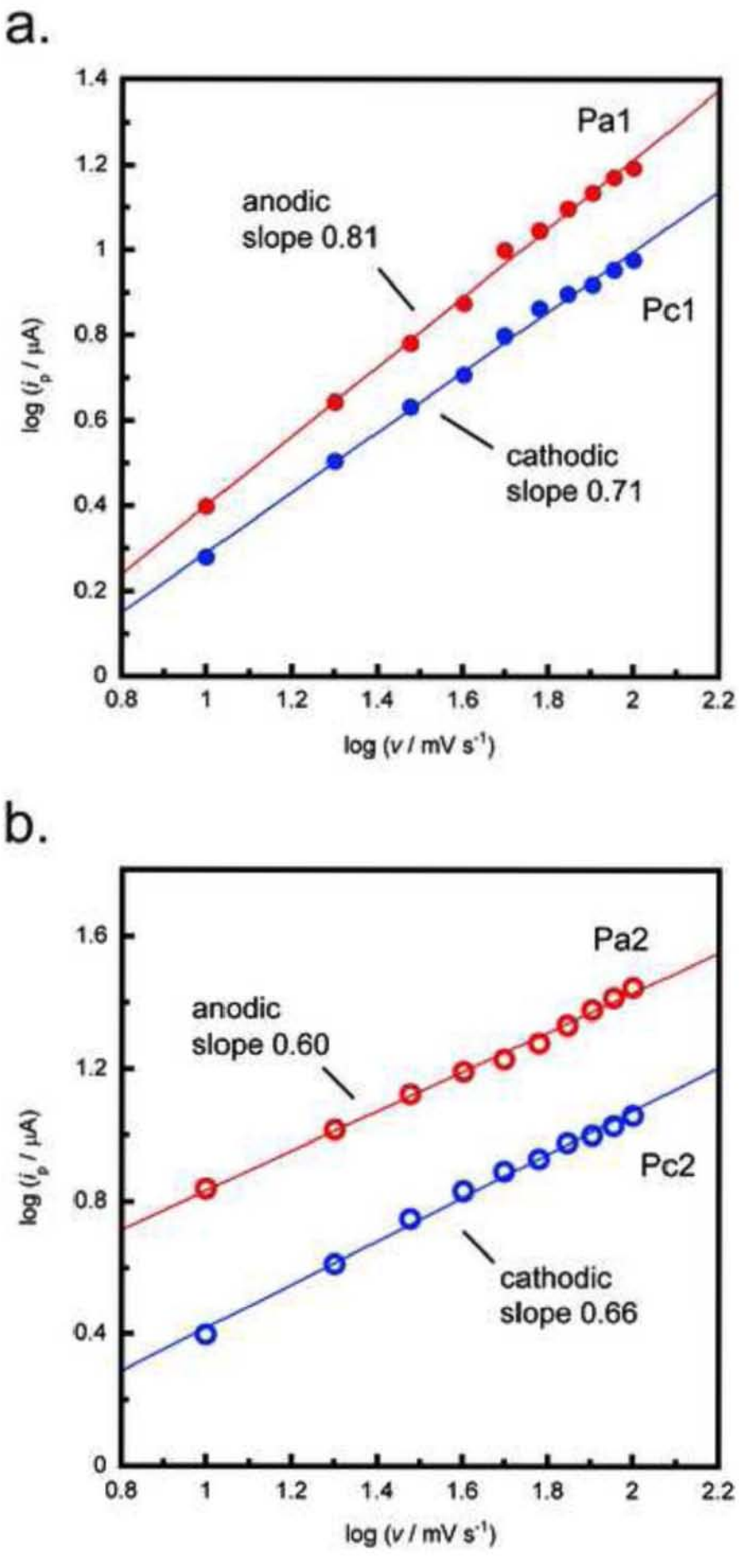

Figure 4 (single column)

Results of potential step chronoamperometry also demonstrated the first-order phase transition nature for both steps (Fig. 4). Referring to the peak potentials at 0.1 mV s^{-1} in Fig. 2, applied potential steps were programmed to take jumps over the peaks noted in each of the panels. The equilibration time at the initial potential was always set over 10 s to reach a constant residual current. Transient currents were the sum of the double-layer charging current and faradaic current due to the redox reaction of viologens. The non-faradaic double-layer charging current associated with the phase change is minor at a HOPG electrode [1,22-24]. In each panel a through e in Fig. 4, a current hump accompanied by a current peak (for example, at 2 ms in c and 11 ms in e) was observed. This is a demonstration of the occurrence of first-order phase transitions obeying the NGC type kinetics. Transients in the panels b and c exhibited two successive humps, reflecting the potential jumps over the two-step transition, while two-step feature was not obvious in panel e.

3.3. *Bromide concentration dependence of the two-step transition*

In order to describe Br^- concentration dependence of the phase transition processes of dBV, two different experimental strategies were employed. In the first one (Experiment I), solutions of "0.1 mM dBV^{2+} $2Cl^-$ + C_{KCl} KCl + C_{KBr} KBr" were used where the total concentration C_{KCl} + C_{KBr} was kept constant at 0.30 M. Using this solution, we eliminated the influence of ionic strength change of the solution while gained an opportunity to see the effect of coexistent Cl^-. In the second one (Experiment II), solutions of "0.1 mM dBV^{2+} $2Br^-$ + C_{KBr} KBr (10 mM $\leq C_{KBr} \leq$ 1000 mM)" were used in which Cl^- was completely excluded.

Figure 5 shows typical CVs obtained in Experiment I.

Figure 5 (double column)

When $C_{KBr} \leq$ 75 mM in Experiment I, only one pair of sharp peaks was observed as represented by Fig. 5-a, indicative of the occurrence of a single-step faradaic phase transition between a gas-like adsorption layer and a 2D condensed monolayer. Likewise, results of Experiment II at $C_{KBr} \leq$ 75 mM exhibited the single-step transition feature (not shown here) being indistinguishable from Fig. 5-a.

Figure 4

Click here to download high resolution image

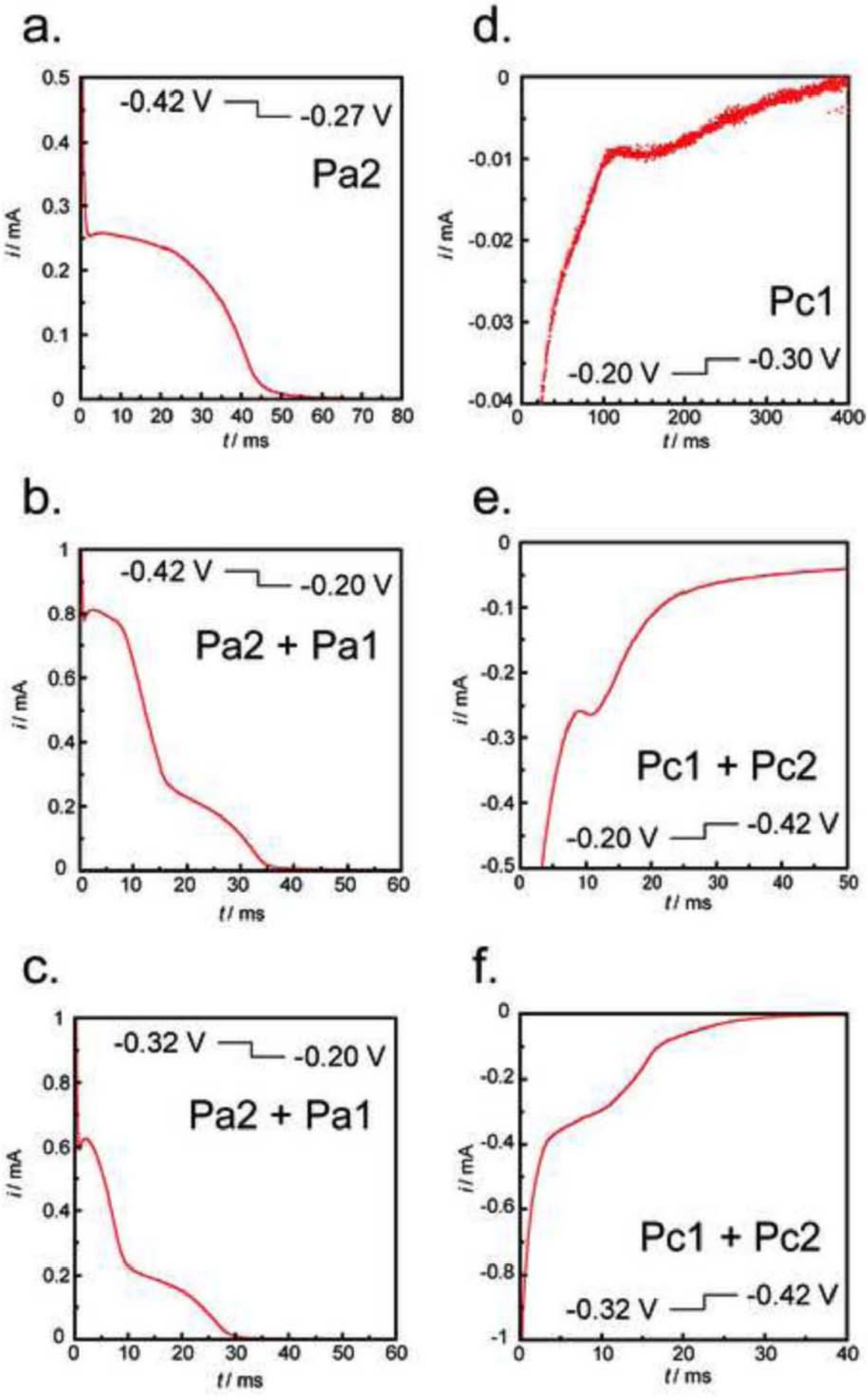

Figure 5
Click here to download high resolution image

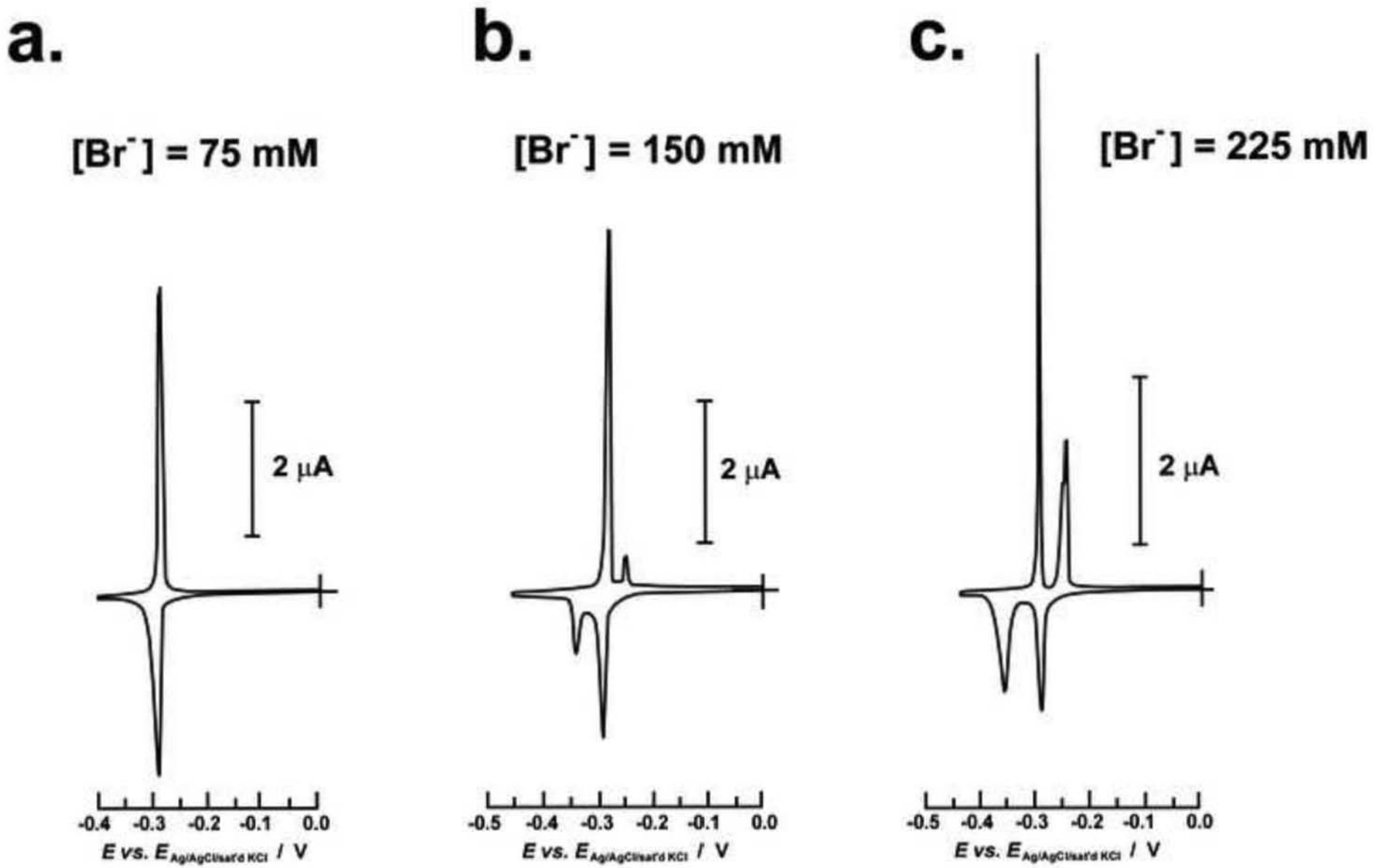

When C_{KBr} exceeded 75 mM, the two-step transition emerged in both Experiments I and II. The coexistent Cl^- neither inhibited nor enhanced the occurrence of two-step transition. Also, the ionic strength of the electrolyte solution showed inconsiderable effect.

Note that CV in Fig. 5-b was the typical pattern of voltammograms in the range of 75 mM < C_{KBr} < 180 mM. As opposed to Fig. 1-b (C_{KBr} = 0.30 M), the peak charge of each redox couple was not balanced so that we obtained relations Γ(Pc1) > Γ(Pa1) and Γ(Pc2) < Γ(Pa2). The transition processes in this concentration range will be discussed later in this section in more detail. On the other hand, CV in Fig. 5-c was typical at $C_{KBr} \geq$ 180 mM, as well as in Fig. 1-b. Equality of both Γ(Pc1) = Γ(Pa1) and Γ(Pc2) = Γ(Pa2) was held in this concentration region.

Figure 6 (single column)

The Br^- concentration dependencies of CV characteristics at 5 mV s^{-1} are summarized in Fig. 6. Values of E_p (Fig. 6-a) and Γ (Fig. 6-b) at four peaks are shown both in the presence of Cl^- (w/Cl^-) and in the absence (w/o Cl^-). As for the E_p values to be plotted, all the measured CVs for different samples were used, while for the Γ values, averages of at least three CVs for different samples were used. The sample-to-sample variability of E_p (with measurement resolution of 2 mV) and Γ under otherwise same conditions were no greater than 13 mV and 0.2 × 10^{-10} mol cm^{-2}, respectively, indicating that influence of HOPG surface defect density is negligibly small compared to the changes with concentration.

In light of Figs. 5 and 6, we can list several important pieces of information about the two-step phase transition.

(i) When C_{KBr} exceeded 75 mM, new peaks Pa1 and Pc2 appeared. When C_{KBr} exceeded 180 mM, two redox couples, Pc1-Pa1 and Pc2-Pa2, became distinct so that the two values of Γ(Pc1) = Γ(Pa1) and Γ(Pc2) = Γ(Pa2) are constant.

(ii) With further increasing concentration of Br^- up to 1.0 M, Pc1-Pa1 couple monotonically shifted to positive, while Pc2-Pa2 shifted to negative (For typical CVs of Experiment II up to 1.0 M KBr, see Supporting Information, Fig. S2).

(iii) At C_{KBr} < 75 mM, the coexistence of Cl^- affected E_{pa} slightly. Except for that, Cl^- had negligible influence over the peak potentials and the Γ values. Because little or no difference between Experiments I and II was found, we concluded that Br^- played a predominant role for

Figure 6
Click here to download high resolution image

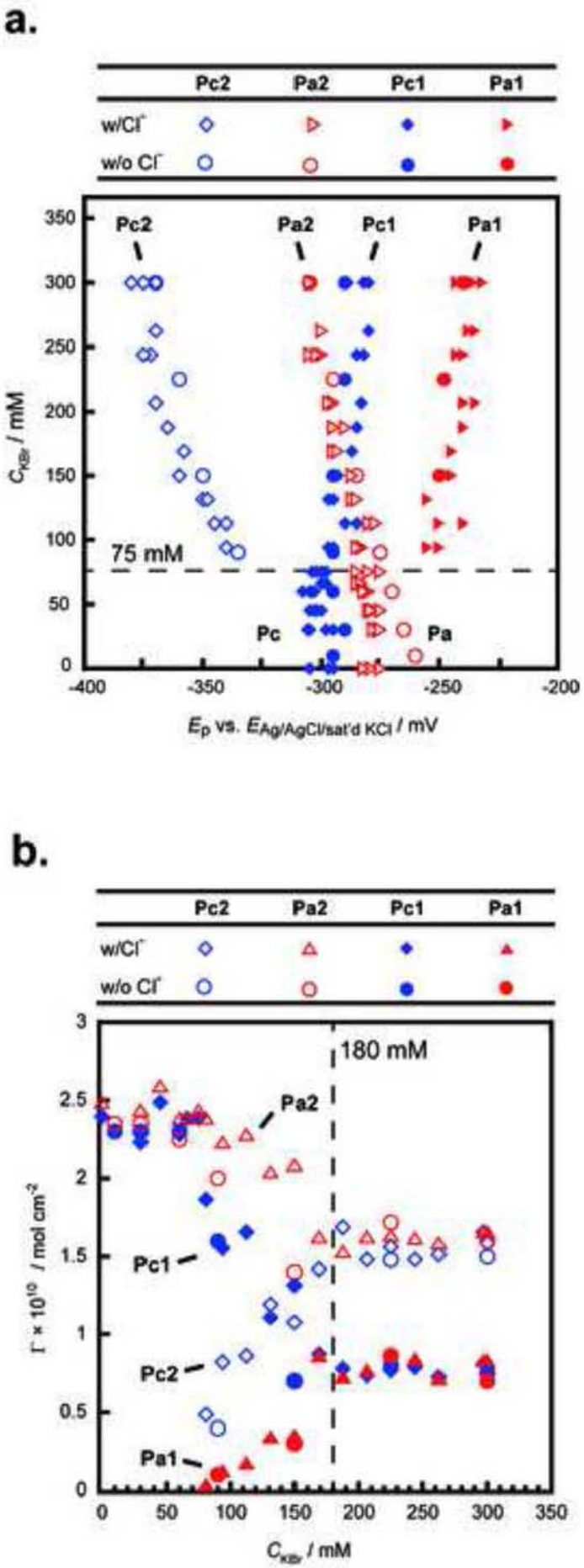

the two-step transition.

(iv) With increasing of C_{KBr} in the range of 75 mM < C_{KBr} < 180 mM, both Γ(Pc1) and Γ(Pa2) decreased whereas both Γ(Pc2) and Γ(Pa1) increased. In the same range, the relations of Γ(Pc1) > Γ(Pa1) and Γ(Pc2) < Γ(Pa2) held, indicating that $dBV^{\bullet+}$ molecules produced at Pc1 should be largely reoxidized at Pa2 but not only at Pa1.

Above (i) and (iv) revealed that the transition process of dBV progressively shifted from a single-step transition to a complete two-step transition with increasing of C_{KBr}, while a single-step voltammetric response was never observed for C_{KBr} > 75 mM. The fact of (i) allows us to assume the presence of a mesophase at C_{KBr} > 75 mM as an intermediate phase between the gas-like adsorption state of dBV^{2+} and 2D condensed monolayer of $dBV^{\bullet+}$. Now we name the three phases with their superficial densities (d, in mol/cm^2) as:

Phase-Ox: gas-like adsorption state of dBV^{2+}

Phase-M: mesophase of $dBV^{\bullet+}$, $d_M = 0.7 \times 10^{-10}$ mol cm^{-2}

Phase-Red: 2D condensed monolayer of $dBV^{\bullet+}$, $d_C = 2.3 \times 10^{-10}$ mol cm^{-2}

Phase-M, whose d value (d_M) is equated to Γ(Pc1) = Γ(Pa1) at C_{KBr} > 180 mM, is stable in the potential range from Pc1 to Pc2 in the negative potential scan and also in the range from Pa2 to Pa1 in the positive scan. In the negative scan, transformation from Phase-M to Phase-Red is accompanied by concurrent adsorption of newly reduced $dBV^{\bullet+}$ to be incorporated into the Phase-Red. When C_{KBr} > 180 mM, the Phase-M covers the entire HOPG surface in the intermediate potential region. The Phase-Red covers the entire surface in the condensed phase potential region at any C_{KBr}.

When C_{KBr} < 75 mM, the Phase-M does not exist. Therefore, a single-step transition between Phase-Ox and Phase-Red takes place, and Phase-Red covers the entire HOPG surface at negative potentials than the transition potentials.

In the range of 75 mM < C_{KBr} < 180 mM, in light of the above fact of (iv), we can model the following scenario. Starting from Phase-Ox, the reduction process at peak Pc1 produces Phase-M and Phase-Red simultaneously covering the entire HOPG surface with area fractions of θ_M and θ_C (= 1 − θ_M), respectively. After the Peak Pc2, the Phase-Red exclusively covers the entire surface. Therefore, Pc2 involves two processes: transition of Phase-M to Phase-Red and additional reductive adsorption of $dBV^{\bullet+}$ to be incorporated into Phase-Red. Shrinking of pre-existing $dBV^{\bullet+}$ adsorption area in the former process allows for the latter process to finally

cover the entire surface with Phase-Red. At the peak Pa2, a portion of Phase-Red changes to be Phase-M with an area fraction of θ_M', and simultaneously in the other part, oxidative transformation from Phase-Red to Phase-Ox takes place. Finally at the peak Pa1, Phase-M is oxidized back to Phase-Ox. Importantly, the structure and superficial $dBV^{\bullet+}$ density of Phase-M is invariant with Br^- concentration in solution.

Based on this scenario, keeping in mind that the interconversion between Phase-M and Phase-Red is not associated with current, we can write:

$$\Gamma(\mathrm{Pc1}) = d_M\theta_M + d_{RED}\theta_C = d_M\theta_M + d_{Red}(1 - \theta_M) = d_{Red} - \theta_M(d_{Red} - d_M) \quad (3)$$

$$\begin{aligned}\Gamma(\mathrm{Pc2}) &= d_{Red}[1 - \theta_C - \theta_M(d_M/\, d_{Red})] = d_{Red}[1 - (1 - \theta_M) - \theta_M(d_M/\, d_{Red})] \\ &= d_{Red}\theta_M[1 - (d_M/\, d_{Red})] = \theta_M(d_{Red} - d_M)\end{aligned} \quad (4)$$

$$\Gamma(\mathrm{Pa2}) = d_{Red} - d_M\theta_M' \quad (5)$$

$$\Gamma(\mathrm{Pa1}) = d_M\theta_M' \quad (6)$$

Figure 7 shows plots of the surface fraction values of Phase-M (θ_M and θ_M') obtained from Fig. 6-b by the use of Eqs. (3) through (6). The values of θ_M obtained from Eqs. (3) and (4) are in good agreement. This is also the case for the values of θ_M' obtained from Eqs. (5) and (6). In the range of 75 mM < C_{KBr} < 180 mM, θ_M is higher than θ_M'. At Pa2, the transition from Phase-Red to Phase-Ox is the major process compared to that from Phase-Red to Phase-M. At C_{KBr} > 180 mM, both θ_M and θ_M' reach unity. Taken together, the data sets in Fig. 6 and 7 are consistent with the aforementioned scenario, and θ_M is controlled by C_{KBr}, while the sums of both Γ(Pc1) + Γ(Pc2) and Γ(Pa1) + Γ(Pa2) are unchanged. The superficial density of Phase-M, d_M, is a constant. The remaining question is the molecular ordering structure of $dBV^{\bullet+}$ Br^- in Phase-M with d_M.

Figure 7 (single column)

Figure 7
Click here to download high resolution image

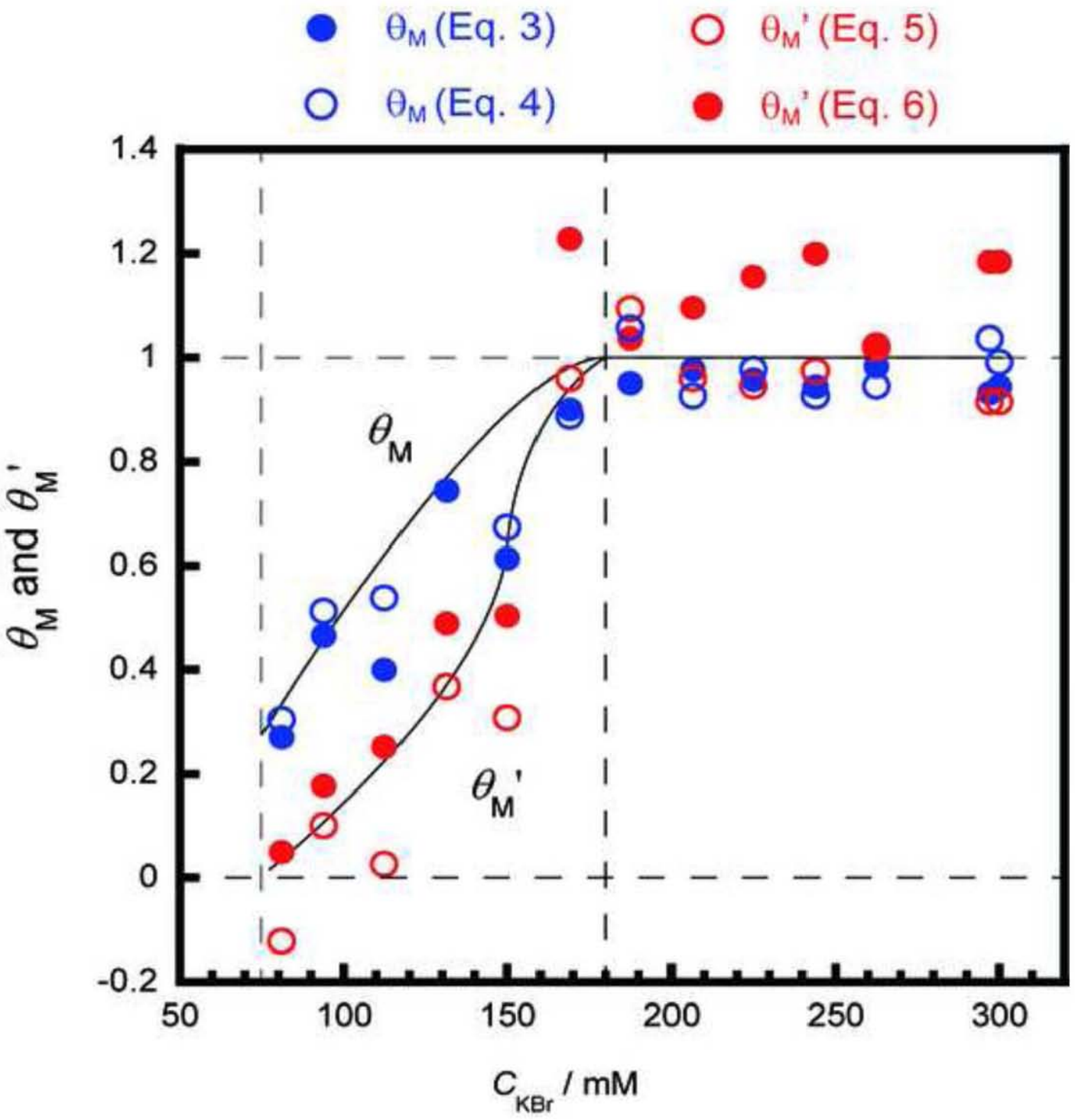

3.4. *Electroreflectance approach to two-step transitions*

Results of voltammetric measurements pointed to the existence of three phases. In 0.30 M KBr, the HOPG electrode surface is always covered with a unique phase, one out of Phase-Ox, Phase-M, and Phase-Red. We conducted ER spectral measurements at this concentration in order to the explicitly distinguish the state of molecules in these three phases.

In the ER measurements, we set E_{dc} near the boundary of adjacent two different phases so that the range of potential modulation, $E_{dc} \pm \Delta E_{ac}$, well overlaps the two phases but not three. Then, ER spectrum (ERS) represents in principle the difference reflectance spectrum between the two phases [20]. The Phase-Ox is colorless in the wavelength range used in the present ER measurements. The ERS at the Phase-Ox/M boundary should represent the difference reflectance spectrum between Phase-Ox-covered HOPG only with dBV^{2+} and Phase-M-covered HOPG only with $dBV^{\bullet+}$of this phase. The ERS at the Phase-M/Red boundary should represent the difference reflectance spectrum between Phase-M-covered HOPG only with $dBV^{\bullet+}$ of this phase and Phase-Red-covered HOPG only with $dBV^{\bullet+}$ of this phase, plus the contribution from additional incorporation of on-site reduced $dBV^{\bullet+}$ into Phase-Red.

Figure 8 (single column)

Figure 8 shows ER spectra at an HOPG electrode in 0.1 mM dBV^{2+} $2Cl^-$ + 0.30 M KBr solution. In Fig. 8-a, $E_{dc} = -257$ mV was slightly more positive than $E_{P1,1/2} = -268$ mV, and $E_{dc} \pm \Delta E_{ac}$ ($\Delta E_{ac} = 57$ mV) covered only the Phase-Ox/M interconversion. On the comparison basis in reference to the faradaic phase transitions at HOPG of heptyl viologen [1] and dBV in KCl solution [8], this ERS represents the reflectance spectral difference between "a dBV^{2+} layer (Phase-Ox)-covered HOPG surface" and "an HOPG surface in direct contact with strongly light-absorbing $dBV^{\bullet+}$ layer (Phase-M)". Because the former layer is colorless, the ERS dominantly mirrors the reflectance spectrum of Phase-M on a HOPG surface.

It is worthwhile to compare this ERS with that for dBV in KCl solution [8]. The latter mirrors the reflectance spectrum of the $dBV^{\bullet+}$ condensed monolayer (Phase-Red) on a HOPG surface, because the transition is a single-step. The comparison made us aware that: (i) the peak wavelength of the negative-going band in the mid visible region is shifted from 530 nm in KCl to

Figure 8
Click here to download high resolution image

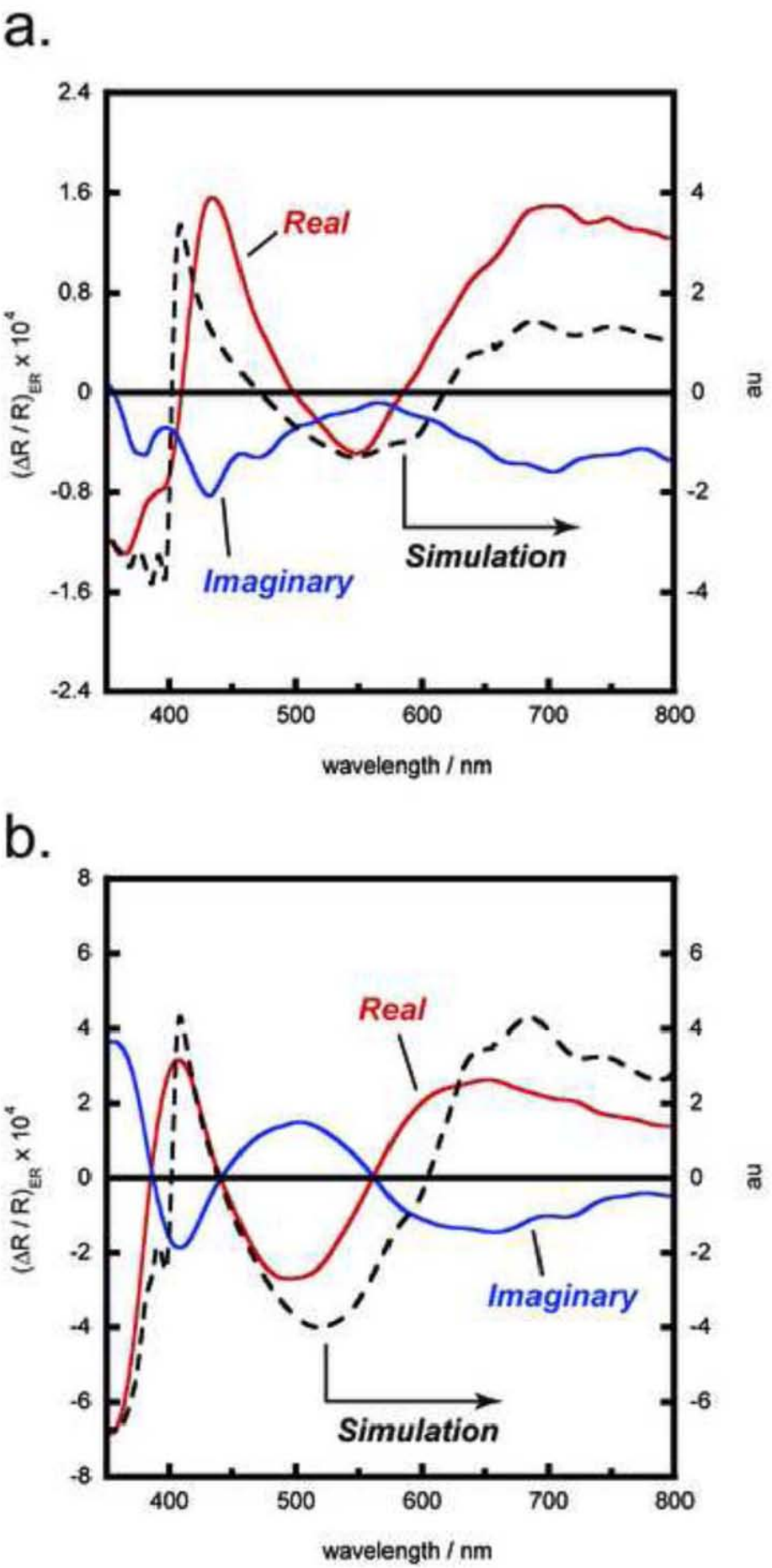

548 nm in KBr, (ii) the wavelength of zero-ER signal is shifted from 469 nm to 498 nm. These differences indicate that the molecular adsorption structure of $dBV^{\bullet+}$ in Phase-M in the presence of Br^- is different from that in Phase-Red condensed phase in the absence of Br^-.

To highlight the difference between Phase-M and Phase-Red, comparison of experimental ERS with simulated ones is helpful. ERS simulation was made as described previously [1] by the uses of solution absorption spectra of $dBV^{\bullet+}$ (see Supporting Information Fig. S3), Kramers-Kronig transformation calculation, and three-phase stratified optical model.

The dashed line in Fig. 8-a (for the same curve, see Fig. S4, dashed line) is an ERS simulated by the use of the solution absorption spectrum of $dBV^{\bullet+}$ monomer (see Fig. S3, dashed line). In the simulation, the state of the positive side of the potential modulation is an HOPG surface fully covered with Phase-Ox and that at the negative side is an HOPG surface covered with a monolayer of $dBV^{\bullet+}$ monomer with flat-lying orientation of its longitudinal bipyridinium axis. This simulation qualitatively reproduced the experimental spectrum (Fig. 8-a, solid line). We also used the solution absorption spectrum of $dBV^{\bullet+}$ dimer (see Fig. S3, solid line) in the simulation. Thus obtained dimer-based simulated ERS (see Fig. S4, solid line and Fig. S5, dashed line) was dissimilar to the experimental ERS in Fig. 8-a for Phase Ox/M interconversion. We may conclude, therefore, that $dBV^{\bullet+}$ molecules in the Phase-M are of a monomer state but not of a dimer-like face-to-face π-stacked state, in contrast to Phase-Red for $dBV^{\bullet+}$ molecules on HOPG in KCl solution [8].

The experimental ERS in KCl solution [8] (see Fig. S5, solid lines) showed high resemblance to the simulated ERS (see Fig. S5, dash line for real part) using the dimer absorption spectrum. The experimental negative going real-part signal in KCl solution at 530 nm was well in accord with the simulated spectrum (see Fig. S5). In contrast, the experimental wavelengths of zero-ER signal (469 nm and 582 nm) were different from 447 nm and 604 nm in simulated spectrum (see Fig. S5). This difference may arise from the difference of the absorption band of $dBV^{\bullet+}$ between its 2D condensed monolayer on the electrode surface and $dBV^{\bullet+}$ dimer in aqueous solution. The simulated ERS (see Fig. S4, solid line and Fig. S5 dashed line) using an absorption spectrum of $dBV^{\bullet+}$ dimer is quite useful as a reference spectrum to monitor the state of a 2D condensed monolayer.

The experimental ERS in Fig. 8-b represents exclusively the Phase-M/Red interconversion potential domain, as being verified from the used values of E_{dc} and ΔE_{ac}. At the positive side of

the potential modulation, we have a Phase-M-covered electrode with a superficial density of d_M plus dBV^{2+} in the proximity to the electrode surface as a precursor of $dBV^{\bullet+}$ to be incorporated in Phase-Red. At the negative side, we have a Phase-Red-covered electrode with d_C ($>d_M$).

The experimental ERS in Fig. 8-b clearly showed that a $dBV^0/dBV^{\bullet+}$ redox process is not included. To see as to whether this spectrum exhibited reorientation of pre-existing $dBV^{\bullet+}$ molecules, we made following simulation.

The process at Pc2 involves:

$$dBV^{2+}{}_{soln} + e^- \rightarrow dBV^{\bullet+}{}_{Phase\text{-}Red} \qquad 1.6 \times 10^{-10}\ \text{mol cm}^{-2} \tag{7}$$

$$dBV^{\bullet+}{}_{Phase\text{-}M} \rightarrow dBV^{\bullet+}{}_{Phase\text{-}Red} \qquad 0.7 \times 10^{-10}\ \text{mol cm}^{-2} \tag{8}$$

We first calculated two reflectance spectra. One is for a 0.7/2.3(= 0.7/(0.7+1.6)) = 0.30 ML submonolayer of $dBV^{\bullet+}$ monomer (Phase-M) on a HOPG, representing the positive side of the potential modulation, where ML = monolayer amount. The other is for 1 ML of $dBV^{\bullet+}$ dimer (Phase-Red), representing the negative side of the potential modulation. Then, simulated ER spectral profile was obtained by subtracting the latter reflectance spectrum from the former. The result was shown by the dashed curve in Fig. 8-b (for the same curve, see Fig. S6, solid line). We herein assumed that the colorless oxidized form, dBV^{2+}, contributes not at all to the ER spectral structure. In the experimental spectrum (Fig. 8-b, solid lines), the characteristic wavelengths include a negative-going real part peak at 360 nm, a positive-going real part peak at 408 nm, and a zero-ER signal at 441 nm. These are well in accord with the simulated ERS (Fig. 8-b, dashed lines). A negative-going real part peak wavelength of 498 nm and a zero-ER signal wavelength at 561 nm in the experimental spectrum were different from those in simulated spectra, presumably because of the difference of $dBV^{\bullet+}$ dimer spectrum in adsorption layer from that in aqueous solution.

Separately, we calculated a simulated ERS (see Fig. S6, dashed line) using an absorption spectrum of $dBV^{\bullet+}$ monomer instead of dimer to represent the Phase-Red $dBV^{\bullet+}$ monolayer. That is, we presumed interconversion between 0.30 ML submonolayer of $dBV^{\bullet+}$ monomer (Phase-M) on a HOPG, representing the positive side of the potential modulation, and a full monolayer of $dBV^{\bullet+}$ monomer, representing the negative side of the potential modulation. The result (see Fig. 6S, dashed line) appeared far different from the experimental ERS in Fig. 8-b. Therefore, we conclude that, in Phase-Red, $dBV^{\bullet+}$ molecules form a 2D condensed monolayer as a dimer-like, face-to-face-π-stacked state on the HOPG surface.

3.5. Examination of some other viologens in regards to specific effect of bromide ion

Do benzyl side-groups induce the specific effect of Br^- on the appearance of the two-step transition? As far as previously reported phase transitions on an HOPG electrode surface are concerned, a two-step transition has never been observed for dialkyl viologens, including diheptyl violgen (HV), in 0.30 M KBr solution. Although we examined various C_{KBr} up to 0.50 M with HV, we always recorded single-step transitions to reach condensed monolayers.

Figure 9 (single column)

Further, we used benzyl-heptyl viologen (BHV) in order to examine as to whether introduction of benzyl group at both side of viologen is a prerequisite to realize two-step transition or not. As a result (Fig. 9), BHV exhibited only a single-step transition. Even when extending the negative end potential to more negative to reach the onset of diffusion-controlled bulk redox reaction, no trace of the second step phase transition was observed.

We may conclude that the presence of benzyl groups at both side of the bipyridinium moiety is essential for two-step faradaic phase transition. Most likely, two benzyl groups in a molecule is necessary to stabilize the mesophase, or the presence of alkyl chain at least at one end hinders the production of the mesophase. Even when a bipyridinium moiety has a side-on orientation to the HOPG surface, if both ends benzyl groups have flat-lying orientation, π-π stacking between bipyridinium moieties cannot achieved as in the case of the condensed phase of $dBV^{\bullet+}$. This consideration will be incorporated to model the mesophase in the next section.

3.6. A model for Structures of Phase-M and Phase-Red

We propose a model shown in Scheme 1 with an emphasis on the structure of Phase-M. For simplicity, two concentration ranges of $C_{KBr} < 75$ mM and $C_{KBr} > 180$ mM are highlighted.

When $C_{KBr} < 75$ mM, reduction of a gas-like adsorption layer of dBV^{2+} (Phase-Ox) directly

Figure 9
Click here to download high resolution image

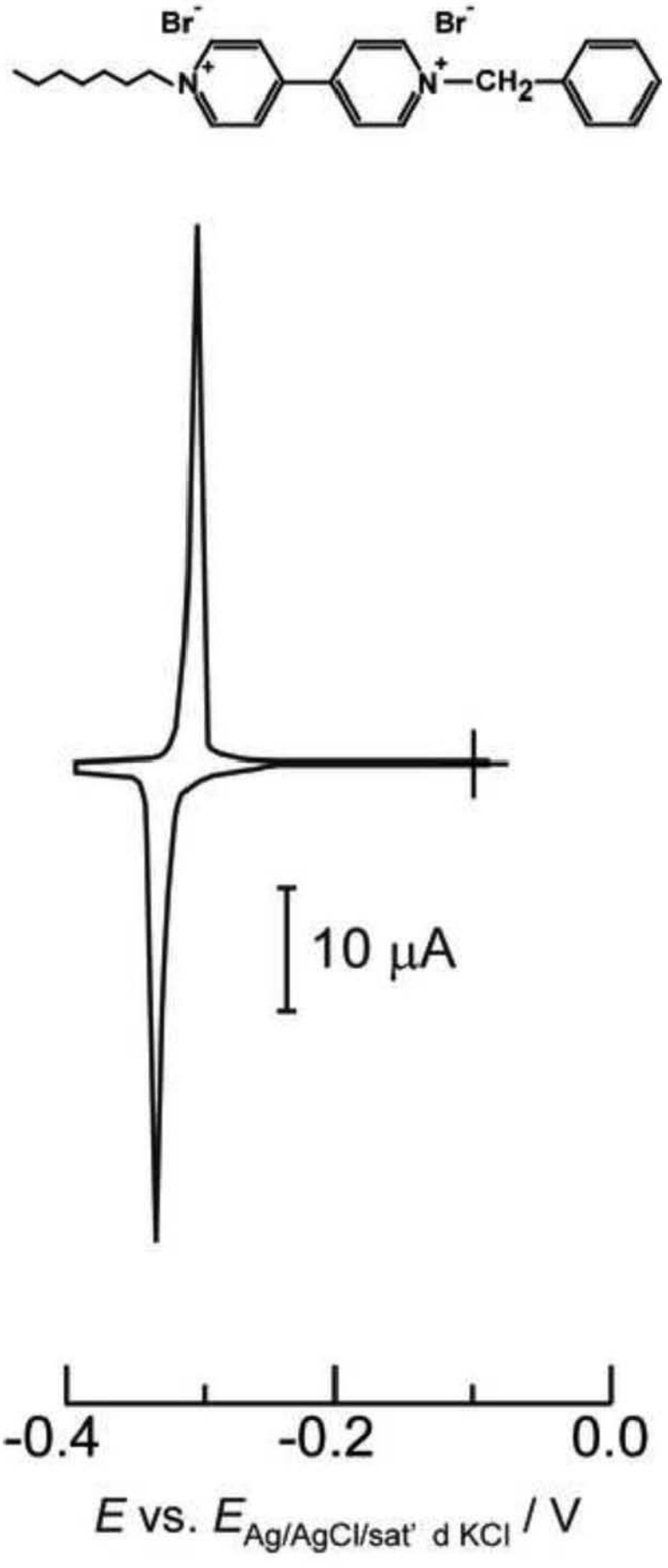

gives a 2D condensed monolayer (Phase-Red) with 0.69 nm^2/molecule, fully covering the HOPG surface. In this layer, the planar bipyridinum cation radial moiety of $dBV^{\bullet+}$ assumes flat-lying orientation of its longitudinal axis with a side-on configuration. The benzyl groups are also oriented with a side-on configuration, allowing close-packing of $dBV^{\bullet+}$ through face-to-face π-π stacking. This single-step phase transition mechanism is the same as that in KCl solution [8].

When $C_{KBr} > 180$ mM, there is a potential region in which a stable mesophase Phase-M fully covers the HOPG surface. As depicted in Scheme 1, we propose a 2D ordered structure of $dBV^{\bullet+}$ Br^- in the mesophase (Phase-M). $dBV^{\bullet+}$ adsorbs with a flat-lying orientation of its longitudinal axis of the side-on bipyridinium moiety, while the orientation of the benzyl groups is a face-on to the HOPG surface. Two benzyl groups in a molecule are in *trans*-conformation, which regulates the inter-ring distance to the neighboring bipyridinium. The directly adsorbed, desolvated Br^- on the HOPG is incorporated into the $dBV^{\bullet+}$ mesophase in a manner being sandwiched by two different bipyridinium moieties. The rows of $dBV^{\bullet+}$–Br^- repeats are arranged in a commensurate structure to other rows. The nearest inter-Br^- distance is 0.78 nm. The area occupied by one $dBV^{\bullet+}$ Br^- is 2.1 nm^2, which is in harmony with the value of d_M.

Scheme 1 (double column)

The rationale behind this model structure includes:

(i) Strongly attractive interaction between the adsorbed species is the requisite of the first order transition. The interaction is mainly achieved by electrostatic attraction between $dBV^{\bullet+}$ moieties and Br^- ions. We estimated the electrostatic potential energy between a pair of $dBV^{\bullet+}$ and Br^- taking the delocalization of positive charge in $dBV^{\bullet+}$ into account based on our DFT calculation. Using the distance between center of $dBV^{\bullet+}$ and Br^- to be 0.39 nm and point charge approximation for Br^-, we obtained −2.07 eV using relative dielectric constant of unity. This value is large enough for the first-order phase transition.

(ii) Br^- triggers the mesophase formation, or Br^- itself is incorporated in the phase. In fact, high concentration of Br^- is the necessary condition.

(iii) The results of ER measurements reveal that the mesophase consists of $dBV^{\bullet+}$ monomers without the π-stacked $dBV^{\bullet+}$ polymer formation. That is, involvement of radical cation dimer components can be excluded as discussed in Section 3.4.

Scheme 1

Click here to download high resolution image

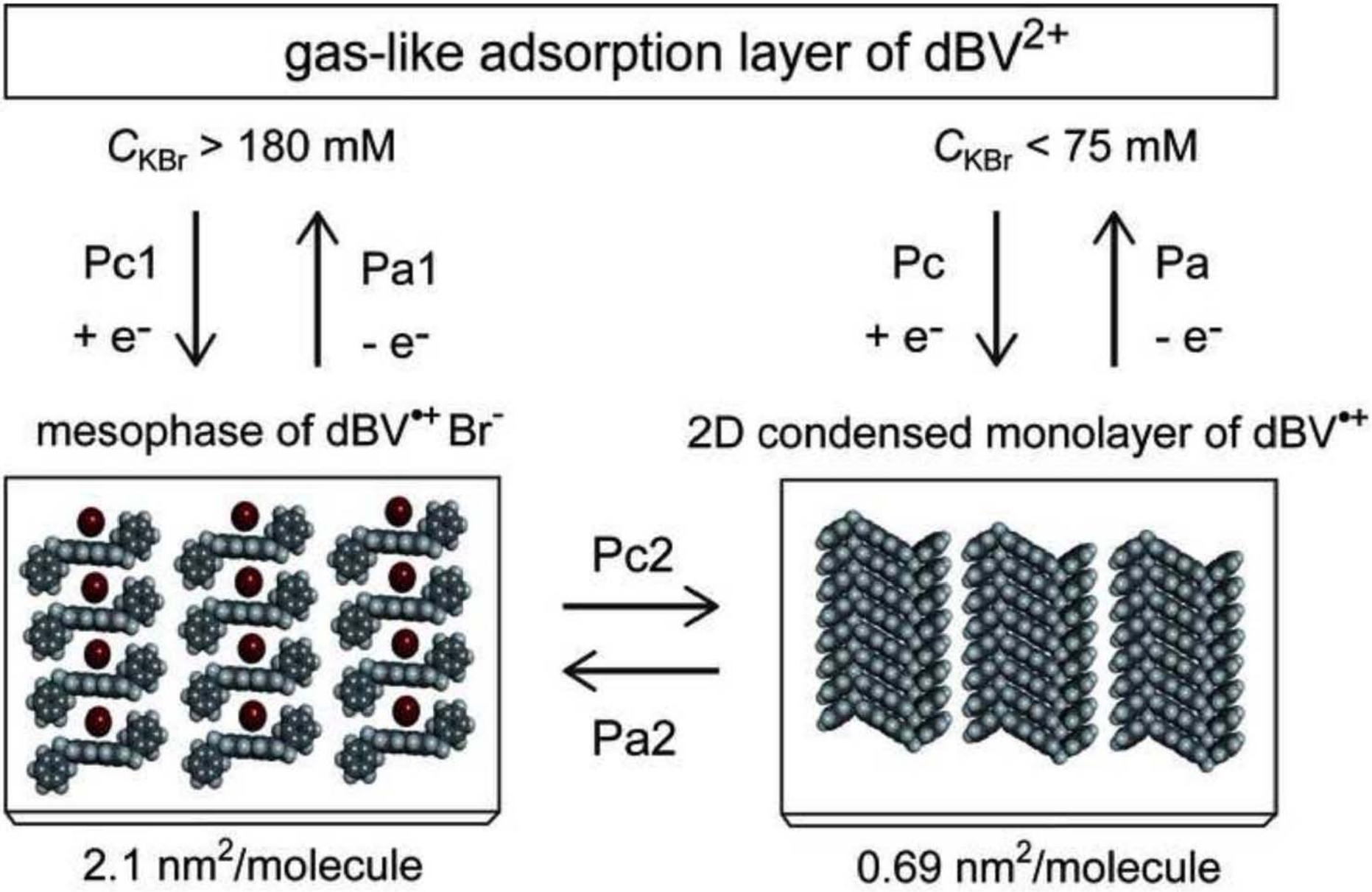

(iv) Using the experimental value of Γ for Phase-M, the area occupied by one $dBV^{\bullet+}$ is approximately 2.1 nm^2/molecule. This can be achieved by a side-on orientation of bipyridinium moiety, oblique but almost flat-laying orientation of benzyl moiety, together with the involvement of desolvated bromide ion.

(v) The presence of benzyl groups at both side of a bipyridinum moiety is essential for two-step transitions. The benzyl groups can separate bipyridinium moieties of $dBV^{\bullet+}$ from each other by steric hindrance. The π-π interaction of a benzyl group with the HOPG surface takes precedence over that with a bipyridinum moiety.

(vi) The face-on adsorption of $dBV^{\bullet+}$ in Phase-M can be readily denied, because the superficial density of such $dBV^{\bullet+}$ is twice of d_M [8].

(vii) Formation of aggregates of $dBV^{\bullet+}$ in Phase-M may be denied, because otherwise we should have observed the broader CV peaks due to the lack of the inhomogeneity in intermolecular interactions required for first-order phase transition. The constant upper limit of experimental total Γ value denies multilayers formation. The phase transition of dBV can be regarded as a UPD process of organic redox species.

The presence of Br^- in Phase-M in between radical cation bipyridinium moieties in a sandwiched manner may be allowed by a lower desolvation energy of Br^- compared to Cl^- (−75.3 kcal/mol for Br^- and −81.3 kcal/mol for Cl^-) [25,26], appropriate ionic diameter (0.36 nm), and high polarizability to stabilize radical cation bipyridinium moiety−Br^- repeats. ER spectral data, especially the difference between Figs. 8a and 8b, revealed that Phase-M is not the partial formation of Phase-Red.

As shown in Scheme 1, one-electron reduction of dBV^{2+} molecules to $dBV^{\bullet+}$ takes place at Pc2 simultaneously with the non-faradaic reorientation of pre-existing $dBV^{\bullet+}$ in Phase-M to Phase-Red. In this process, significant amount Br^- ions should be displaced from the HOPG surface. It is presumably driven in part by the increased electrostatic repulsion of Br^- with the electrode surface negative charge. Also, this displacement facilitates the formation of direct π-stacking structure of both bipyridinium and benzyl moieties of $dBV^{\bullet+}$ as a consequence of rotation of benzyl groups.

Although the model is self-explanatory, it is in part speculative. Thus, the molecules in Phase-M remain to be directly imaged. We tried *in-situ* electrochemical STM imaging, but we

have not yet obtained any reliable molecular level images in Phase-M. Note that in the trials, we did not see any 3D agglomerated molecules. Further efforts to obtain the images are presently still underway.

4. Conclusions

Occurrence of two-step first-order faradaic phase transition of dBV on an HOPG electrode was found in KBr solution. Emergence of a new $dBV^{\bullet+}$ Br^- mesophase was observed at $[Br^-] >$ 75 mM. We proposed an adsorption structure of the mesophase which consists of both $dBV^{\bullet+}$ monomer and directly-adsorbed Br^-. The absence of face-to-face stacking of bipyridinium moieties via π-π interaction in the mesophase was confirmed by ER spectral measurements. In order for the mesophase to fully cover the HOPG surface, $[Br^-]$ should be higher than 180 mM. Specific effect of counter anion, Br^- in particular, upon the ordering structure was demonstrated. On an HOPG, two-step phase transition is uncommon for viologens. Other dialkyl viologens as well as benzyl-heptyl viologen did not exhibit the two-step transition even in KBr solution. The two-step transition of dBV can be regarded as an example of a 2D assembling process characterized by a concerted process of an organic molecule and a counter anion. In general, fine control over the molecular assembling processes such as described in this paper may find future application, for example, to fabrication of a nano-template at a specific potential and a differential electrochemical switching.

Acknowledgements

This work was financially supported by Grant-in-aid for Scientific Research from MEXT, Japan (No. 24550158) and Tokyo Ohka Foundation to T. S., Kato Foundation for Promotion of Science to T. H., Japan Society for the Promotion of Science to T. H. We thank Dr. H. Tahara for his technical assistances.

Appendix A. Supplementary data

Supplementary data associate with this article can be found, in the online version, at doi:_____/j. electacta. 201_____

References

[1] T. Sagara, S. Tanaka, Y. Fukuoka, N. Nakashima, Study of the voltammetric spike response of heptyl viologen at a HOPG electrode horizontally touched to a gas/heptyl viologen aqueous solution interface, Langmuir 17 (2001) 1620-1629.

[2] T. Sagara, S. Tanaka, K. Miuchi, N. Nakashima, Characteristics of faradaic phase transition of an adsorption layer of heptyl viologen at a basal plane HOPG electrode, J. Electroanal. Chem. 524-525 (2002) 68-76.

[3] T. Sagara, K. Miuchi, Double potential step chronoreflectometry approach to bi-stable potential region of the faradaic phase transition of heptyl viologen at a HOPG electrode, J. Electroanal. Chem. 567 (2004) 193-202.

[4] T. Sagara, Y. Fujihara, T. Tada, Molecular structure dependence of the phase transition spike response of viologens at an HOPG electrode using bisviologen and carboxylated viologen, J. Electrochem. Soc. 152 (2005) E239-E246.

[5] Y. Tanaka, T. Sagara, Voltammetric study of two-dimensional phase-transition processes of carboxylated viologens at an HOPG electrode as a typical organization process of molecules possessing multiple interaction sites, Bull. Chem. Soc. Jpn. 80 (2007) 1511-1517.

[6] Y. Tanaka, T. Sagara, Formation of viologen radical cation condensed phase through two-dimensional molecular organization process on an HOPG electrode surface in binary viologen solutions, J. Electroanal. Chem. 619-620 (2008) 65-74.

[7] K. Arihara, F. Kitamura, K. Nukanobu, T. Ohsaka, K. Tokuda, Voltammetric and spectroscopic study of the adsorption of alkyl viologens on a HOPG electrode, J. Electroanal. Chem. 473 (1999) 138-144.

[8] T. Higashi, Y. Shigemitsu, T. Sagara, Faradaic phase transition of dibenzyl viologen on an HOPG electrode surface studied by in situ electrochemical STM and electroreflectance spectroscopy, Langmuir 27 (2011) 13910-13917.

[9] K. Arihara, F. Kitamura, Adsorption states of heptyl viologen on an Au(111) electrode surface

studied by infrared reflection absorption spectroscopy, J. Electroanal. Chem. 550-551 (2003) 149-159.

[10] K. Arihara, F. Kitamura, T. Ohsaka, K. Tokuda, Adsorption structure of the heptyl viologen cation radical on a mercury electrode surface: Voltammetric and in situ infrared reflection absorption spectroscopic studies, J. Electroanal. Chem. 488 (2000) 117-124.

[11] K. Arihara, T. Ohsaka, F. Kitamura, Characteristic cyclic voltammograms of alkyl viologens at single crystal gold electrodes, Phys. Chem. Chem. Phys. 4 (2002) 1002-1005.

[12] M. Jiang, E. Sak, K. Gentz, A. Krupski, K. Wandelt, Redox activity and structural transition of heptyl viologen adlayers on Cu(100), Chem. Phys. Chem. 11 (2010) 1542-1549.

[13] J. I. Millán, R. Rodríguez-Amaro, J. J. Ruiz, L. Camacho, Reorientation of the Cation Radical of Heptyl Viologen on Mercury in Water/DMSO Mixed Media, Langmuir 15 (1999) 618-623.

[14] J. I. Millán, J. J. Ruiz, L. Camacho, R. Rodríguez-Amaro, Two-dimensional phase transition in the electroreduction of heptyl viologen on polycrystalline silver in aqueous media, J. Electroanal. Chem. 497 (2001) 168-171.

[15] J. I. Millán, M. Sánchez-Maestre, L. Camacho, J. J. Ruiz, R. Rodríguez-Amaro, Study of the two-dimensional phase formed by salts of the cation radical of heptyl viologen on mercury in aqueous media, Langmuir 13 (1997) 3860-3865.

[16] M. Röefzaad, M. Jiang, V. Zamlynny, K. Wandelt, Potential dependent structure transitions of heptyl viologen layers on Cu(100) studied by in situ STM and IRRAS, J. Electroanal. Chem. 662 (2011) 219-228.

[17] S. L. Tsay, J. S. Tsay, T. Y. Fu, P. Broekmann, T. Sagara, K. Wandelt, Molecular structures of dicarboxylated viologens on a Cu(100) surface during an ongoing charge transfer reaction, Phys. Chem. Chem. Phys. 12 (2010) 14950-14959.

[18] M. F. Toney, J. N. Howard, J. Richer, G. L. Borges, J. G. Gordon, O. R. Melroy, D. Yee, L. B. Sorensen, Electrochemical deposition of copper on a gold electrode in sulfuric acid: Resolution of the interfacial structure, Phys. Rev. Lett. 75 (1995) 4472-4475.

[19] E. Herrero, L. J. Buller, H. D. Abruña, Underpotential deposition at single crystal surfaces of Au, Pt, Ag and other materials, Chem. Rev. 101 (2001) 1897-1930.

[20] T. Sagara, UV-visible Reflectance Spectroscopy of Thin Organic Films at Electrode Surfaces in: R. C. Alkire, D. M. Kolb, J. Lipkowski, P. N. Ross (Eds.) Advances in Electrochemical Science and Engineering, vol. 9, Wiley-VCH, Weinheim, 2006, pp. 47-95.

[21] M. S. Maestre, R. Rodríguez-Amaro, E. Muñoz, J. J. Ruiz, L. Camacho, Use of cyclic voltammetry for studying two-dimensional phase transitions: Behaviour at low scan rates, J.

Electroanal. Chem. 373 (1994) 31-37.

[22] K. K. Cline, M. T. McDermott, R. L. McCreery, Anomalously slow electron transfer at ordered graphite electrodes: Influence of electronic factors and reactive sites, J. Phys. Chem. 98 (1994) 5314-5319.

[23] H. Gerischer, An interpretation of the double layer capacity of graphite electrodes in relation to the density of states at the Fermi level, J. Phys. Chem. 89 (1985) 4249-4251.

[24] H. Gerischer, R. McIntyre, D. Scherson, W. Storck, Density of the electronic states of graphite: Derivation from differential capacitance measurements, J. Phys. Chem. 91 (1987) 1930-1935.

[25] Y. Marcus, A. Rashin, A simple empirical model describing the thermodynamics of hydration of ions of widely varying charges, sizes, and shapes, Biophys. Chem. 51 (1994) 111-127.

[26] S. Zhao, Z. Jin, J. Wu, New theoretical method for rapid prediction of solvation free energy in water, J. Phys. Chem. B 115 (2011) 6971-6975.

Figure Legends

Fig. 1. Cyclic voltammograms for an HOPG electrode in the droplet configuration with (a) 0.1 mM dBV^{2+} $2Cl^-$ + 0.30 M KCl and (b) 0.1 mM dBV^{2+} $2Cl^-$ + 0.30 M KBr solutions. Initial potential (E_i) was −0.1 V. (a) potential sweep rate (v) = 5 mV s^{-1} and A = 0.79 cm^2. (b) v = 10 mV s^{-1}, A = 0.50 cm^2.

Fig. 2. Plot of peak potentials (E_p) of four different peaks in the CVs for a HOPG electrode (A = 0.50 cm^2) in contact with 0.1 mM dBV^{2+} $2Cl^-$ + 0.30 M KBr solution as a function of the logarithm of v.

Fig. 3. Plot of the logarithm of peak currents (i_p) in cyclic voltammograms for a HOPG electrode (A = 0.50 cm^2) in contact with 0.1 mM dBV^{2+} $2Cl^-$ + 0.30 M KBr solution as a function of the logarithm of v. (a) Pc1 and Pa1. (b) Pc2 and Pa2.

Fig. 4. A collection of typical current transient curves in response to single potential step for an HOPG electrode (A = 0.50 cm^2) in the droplet configuration with 0.1 mM dBV^{2+} $2Cl^-$ + 0.30 M KBr solution. Initial/final potential combinations were: (a) −0.42 V/−0.27 V; (b) −0.42 V/−0.20

V; (c) −0.32 V/−0.20 V; (d) −0.20 V/−0.30 V; (e) −0.20 V/−0.42 V; (f) −0.32 V/−0.42 V. In each panel, given is(are) the label(s) of the peak(s) over which potential step was applied.

Fig. 5. Cyclic voltammograms for an HOPG electrode (A = 0.50 cm^2) in the droplet configuration at v = 5 mV s^{-1} with 0.1 mM dBV^{2+} 2Cl$^-$ containing (a) C_{KCl} = 225 mM and C_{KBr} = 75 mM, (b) C_{KCl} = C_{KBr} = 150 mM, (c) C_{KCl} = 75 mM and C_{KBr} = 225 mM.

Figure 6. (a) Plot of E_p at v = 5 mV s^{-1} as a function of C_{KBr} for both Experiments I and II. (b) Plot of CV peak charges in the molecular amounts (Γ) at v = 5 mV s^{-1} as a function of C_{KBr}. For the plot marks in both (a) and (b), see the Table at the top of the figure. Both CV data in the presence of Cl$^-$ (w/Cl$^-$) and in the absence (w/o Cl$^-$) are shown.

Figure 7. Plots of values of the surface fraction of Phase-M (θ_M and θ_M') from four Eqs. (3) through (6) in the text. For the plot marks, see the top of the figure. The thick line was added for a guide for eyes.

Fig. 8. Electroreflectance spectra of an HOPG electrode in a H-M configuration on 0.1 mM dBV^{2+} 2Cl$^-$ + 0.30 M KBr solution. Solid lines are experimental real (red) or imaginary (blue) parts. Dashed lines are spectral curves of real part obtained by simulation (see text for details). (a) E_{dc} = −257 mV, ΔE_{ac} = 57 mV, and f = 14 Hz. (b) E_{dc} = −352 mV, ΔE_{ac} = 71 mV, and f = 14 Hz.

Fig. 9. Cyclic voltammograms for an HOPG electrode (A = 0.50 cm^2) in the droplet configuration with 0.1 mM BHV^{2+} 2Br$^-$ + 0.30 M KBr solution at v = 50 mV s^{-1}. Molecular structure of BHV^{2+} 2Br$^-$ is shown on top of the figure.

Scheme 1. Proposed model structures for mesophase (Phase-M) and 2D condensed phase (Phase-Red) in the two-step faradaic phase transition of dBV on an HOPG electrode surface.